CHALMERS
UNIVERSITY OF TECHNOLOGY

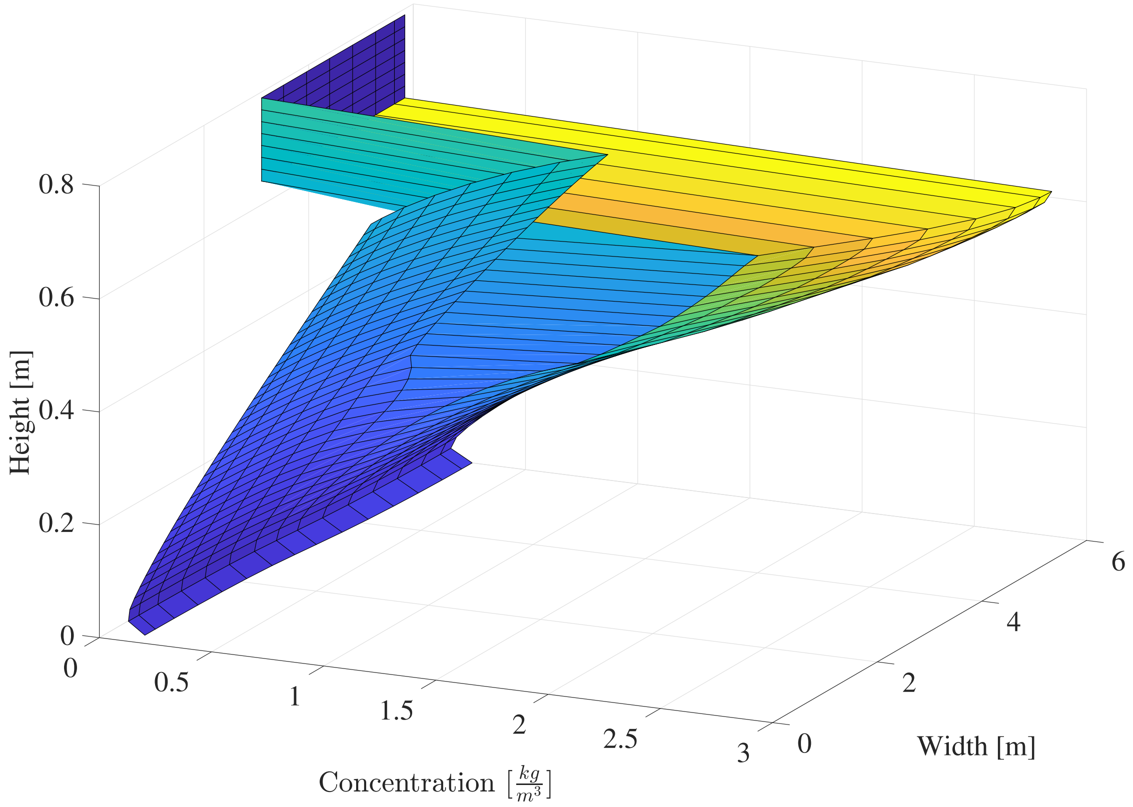

Modeling of Biomass Flow in a Novel Multi-staged Fluidized Bed Concept

Master's thesis in the programme Innovative and Sustainable Chemical Engineering

MARTIN JOHANSSON

Department of Space, Earth and Environment
CHALMERS UNIVERSITY OF TECHNOLOGY
Gothenburg, Sweden 2018

Master's thesis

Modeling of Biomass Flow in a Novel Multi-staged Fluidized Bed Concept

Development of a model describing the axial mixing of biomass in fluidized beds

MARTIN JOHANSSON

Department of Space, Earth and Environment
Division of Energy Technology
Chalmers University of Technology
Gothenburg, Sweden 2018

Modeling of Biomass Flow in a Novel Multi-staged Fluidized Bed Concept
Development of a model describing the axial mixing of biomass in fluidized beds
MARTIN JOHANSSON

© MARTIN JOHANSSON, 2018.

Supervisor: David Pallarès, Department of Space, Earth and Environment
Examiner: David Pallarès, Department of Space, Earth and Environment

Master's Thesis 2018
Department of Space, Earth and Environment
Division of Division Energy Technology
Chalmers University of Technology
SE-412 96 Gothenburg
Telephone +46 31 772 1000

Cover: Concentration profile for all char conversion classes added together.

Typeset in LaTeX
Printed by Chalmers Reproservice
Gothenburg, Sweden 2018

Modeling of biomass flow in a novel multi-staged fluidized bed concept
MARTIN JOHANSSON
Department of Space, Earth and Environment
Chalmers University of Technology

Abstract

A mathematical description of the axial mixing of biomass in bubbling fluidized beds was developed and implemented into an already existing mathematical model. Based on the developed model the performance of novel multi-staged fluidized bed concept was investigated. The novel concept works by inserting a chamber into an already existing unit and in that way introducing two reaction zones that can communicate with each other via a slit at the bottom of the walls delimiting the reaction zones. The implementation of the novel concept enables pyrolysis and char conversion to occur in separate environments.

Based on simulations it was shown that the results are very sensitive to the pyrolysis kinetics, why more studies of the kinetics would be of interest. Furthermore, it was shown that novel concept could be controlled by varying the pressure difference between the reaction zones. The fluidization velocity could also be used as a means for control, but for too big slit heights, the novel concept becomes insensitive to changes in fluidization velocity.

Keywords: Fluidization, Gasification, Combustion, Biomass, Modeling

Acknowledgements

First of all, I would like to extend my gratitude to my examiner and supervisor David Pallarès for entrusting me with this master's thesis, but most of all for the guidance I have received throughout the course of the thesis. His pedagogical way of explaining advanced concepts has been instrumental for my work during the past semester.

I would also like to thank Christer Gustavsson and Anton Larsson for their reinvigorating and inspiring enthusiasm for the novel concept and for taking an interest in my workings.

Furthermore, I would like to thank Anna Köhler for kindly assisting me in my work and for letting me get an insight into her doctoral studies workings. Without it I most definitely would have had a much harder time finalizing my master's thesis.

Martin Johansson, Gothenburg, June 2018

Contents

List of Figures **xi**

List of Tables **xiii**

List of symbols **xv**

1 Introduction **1**
- 1.1 Aim . . . 2
- 1.2 Scope . . . 2
- 1.3 Method . . . 2

2 Theory **3**
- 2.1 Fluidized bed technology . . . 3
- 2.2 Conversion of solid fuels . . . 5
- 2.3 The novel concept . . . 6
- 2.4 Mixing in bubbling fluidized beds . . . 7
  - 2.4.1 Bubble motion . . . 8
  - 2.4.2 Fuel motion in bubble phase . . . 9
  - 2.4.3 Fuel motion in emulsion phase . . . 10
  - 2.4.4 Formation of endogenous bubbles . . . 11

3 Modeling **13**
- 3.1 Modeling . . . 13
- 3.2 Finite volume method . . . 14
- 3.3 Mass transfer between phases . . . 17
- 3.4 Classes . . . 18
- 3.5 Modeling of chemistry . . . 19
- 3.6 Governing equations . . . 21
- 3.7 Fuel mass balance algorithm . . . 22

4 Simulations **23**
- 4.1 Concentration profiles of individual classes . . . 24
- 4.2 Surface loading . . . 24
- 4.3 Sensitivity analysis . . . 25

5 Results and discussion **27**
- 5.1 Concentration profiles of individual classes . . . 27

5.2 Surface loading 30
5.3 Sensitivity analysis 31

6 Conclusion **35**

Bibliography **37**

A Appendix 1 **I**

List of Figures

2.1 Schematic overviw of a CFB boiler (a) and a BFB boiler (b). [7] . . . 4
2.2 Schematic overview of the novel concept, (a) shows a view from above and (b) shows a view from the side. 6
2.3 Schematic overview of the two-phase system, where (a) shows an actual dipiction of a fluidized bed and (b) illustrates how the two phases are defined.[17] 8

3.1 Schematic overview of the overall model structure. 13
3.2 Picture showing how a geometry has been divided into computational cells (a), and a picture illustrating a single computational cell (b). . . 14
3.3 Experimental data from MPT-experiments relating the height in the bed to the probability of mass transfer from the emulsion phase to the bubble phase. 17
3.4 Schematic overview of the concept of classes 19
3.5 Schematic overview of the algorithm for calculating a-coefficients and source terms. 22

4.1 Geometry dimensions used for the simulations 23

5.1 Total concentration profile for all drying an devolatillization classes. . 27
5.2 Total concentration profile for all char conversion classes. 28
5.3 Total concentration profile for all drying and devolatilization classes for fuel particles with an inital diameter of 5mm. 29
5.4 Surface loading for different fuel feed rate into primary chamber. . . . 31
5.5 Sensitivity analysis where the extent of char gasification is related to ΔP, h_{slit} and u_0. Figures (a), (b) and (c) correspond to fluidization velocities of 1.0, 1.2 and 1.4 m/s respectively. 32

List of Tables

3.1 Table showing how a-coefficient is calculated for a one-dimensional problem . . . 16
3.2 Table showing reaction mechanisms for heterogeneous reactions . . . 20
3.3 Table showing reaction mechanisms for homogeneous reactions . . . 20

5.1 Table displaying volumetric gas flow emitted from fuel particles of different sizes. . . . 30

A.1 Table displaying numerical values of parameters used in the model. . . I

List of symbols

A	Pre-exponential factor	
A_0	Area of distributor plate per orifice	$[m^2]$
d_b	Bubble diameter	$[m]$
d_p	Bed solids diameter	$[m]$
E_A	Activation energy	$[J/mol]$
F_B	Buoyancy force	$[N]$
F_D	Drag force	$[N]$
F_G	Gravitational force	$[N]$
F_{Lift}	Lift force due to endogenous bubbles	$[N]$
f_{bub}	Bubble frequency	$[s^{-1}]$
f_w	Wake fraction	$[-]$
g	Gravitational acceleration	$[m/s^2]$
h_{slit}	Height of slit under chamber walls	$[m]$
m_f	Fuel particle mass	$[kg]$
p	Pressure	$[Pa]$
Q	Volumetric flow rate gas emitted from fuel particle	$[m^3/s]$
q_z	Probability for mass transfer	$[-]$
R	Gas constant	$[J/molK]$
u_0	Fluidization velocity	$[m/s]$
u_b	Bubbke rise veloicity	$[m/s]$
u_{br}	Rise velocity of a single bubble	$[m/s]$
u_f	Fuel particle velocity	$[m/s]$
u_{mf}	Minimum fluidization velocity	$[m/s]$
u_{sd}	Downward velocity of solids in the emulsion phase	$[m/s]$
u_{tf}	Throughflow velocity	$[m/s]$
V_b	Bubble volume	$[m^3]$
V_w	Wake volume	$[m^3]$
ΔP	Pressure difference between primary and secondary chamber	$[Pa]$
β	Surface loading	$[-]$
ρ_e	Density of emulsion	$[kg/m^3]$
ρ_f	Fuel density	$[kg/m^3]$
α	Impact factor	$[-]$
δ	Bubble density	$[-]$

1

Introduction

One of the greatest struggles facing the modern society of today is the rapidly changing climate of planet Earth. An overwhelming majority of today's climate scientist agree that these changes can be ascribed to human activity. Therefore, due to increasing anthropogenic emissions, an increase in the severity of the environmental impact have been observed. For instance, Earth's surface temperature has for all decades, starting from 1980 to today, been significantly warmer than any decade between 1850 and 1970 [1].

Since the start of the 21st century, the amount of anthropogenic emissions of CO_2 has increased 3% annually. If this trend is continued, it is expected that the planet's ecosystems will be subjected to a climate change that is both dangerous and irreversible [2]. In order to mitigate the effects of climate change, a significant decrease of anthropogenic CO_2 emissions would be necessary. In light of this, a transition to a society based more on renewable sources of energy would be an important step towards decreasing the amount of anthropogenic CO_2 emissions.

One renewable source of energy is biomass, which often is considered to be CO_2-neutral. This is true when the CO_2 released during combustion of biofuel, equals the amount of CO_2 sequestered in biomass [3]. In the energy field, the most common use of biomass is its conversion to produce heat and energy. Most of the energy in biomass is however stored as volatile matter, which is valuable since it can be used as a precursor to biochemicals, biogas and biofuels for the transport sector. Recently, Chalmers has developed a novel concept in which the volatile matter of biomass can be extracted from fluidized bed combustors.

In essence, the concept works by separating the fluidized bed combustor into two reaction zones by inserting a devolatilization chamber into the already existent unit. The walls delimiting the two reaction zones are submerged in the fluidized bed, but a small slit at the bottom of the walls makes it possible for the two reaction zones to communicate with each other [4]. By having two separate reaction zones, the volatile matter of biomass can be extracted from the devolatilization chamber and the remaining char fraction can then be transported to the secondary chamber to undergo conversion.

1.1 Aim

The aim of the project presented in this thesis is to investigate the performance of a novel multi-staged fluidized bed concept. Since the axial mixing is of great importance for the novel concept, a model describing the axial fuel mixing is to be developed. The developed model is then to be implemented into an already existing three dimensional model for fluidized bed combustors. By performing simulations with the updated version of the model, the novel concepts performance is to be assessed and possible operational parameters that can be used to control the process are to be suggested.

1.2 Scope

The project is specially directed towards the modeling of bubbling fluidized bed combustors and therefore fluidized bed combustors operating at circulating conditions is not considered in this work. Furthermore, the current version of the model only solves mass balances describing the mixing in the bed, i.e. solution of a heat balance is omitted from the project. Little emphasis has been put on the chemistry in the model, instead already implemented models for the chemical kinetics have been used in the work. Finally, all forms of experimental work that could be performed to validate the model falls outside the scope of the project.

1.3 Method

The description of the axial mixing is developed on the basis of empirical and semi-empirical expressions for the motion in fluidized beds. The developed fuel mixing model is then implemented into the existing three dimensional model. The model is constructed in the software MATLAB 2015b developed by MathWorks.

2

Theory

2.1 Fluidized bed technology

Fluidization is a technology utilized for a wide variety of applications ranging from coating of solids to combustion of coal and biomass. The technology's name is derived from the commonalties shared between a fluidized bed and a liquid of low viscosity. For instance, light objects float on the bed surface and if two beds are connected the level of the two beds equalizes [5].

The technology works by letting a fluid pass upwards through a bed of fine particles. If the velocity sufficiently high, the frictional forces between fluid and solids may overcome the weight of the solids and thus suspending the solid particles [5]. The fluidization velocity resulting in equal size of the frictional forces and the weight of the solids, is termed the minimum fluidization velocity (u_{mf}).

Depending on the fluidization velocity a number of different regimes can be defined. Beds operated at low fluidization velocities are called fixed beds and these the fluidization medium percolates through the voids of the beds. Increasing the fluidization velocity further the bed material starts to vibrate and move apart from one another and thus yielding the expanded bed. As the bed reaches u_{mf} the bed is called an incipiently fluidized bed.

Increasing the fluidization velocity beyond u_{mf} leads to the onset of the bubbling fluidized bed regime, which is of special interest for the project presented in this thesis. As the name suggests, large instabilities in form of bubbling and channeling through the bed are induced.

One of the most common application of fluidized beds in the energy sector is combustion for heat and power generation. Introducing a fluidized bed into the combustion unit offers several positive effects on the combustion process. Initially, the concept of fluidized bed combustion was developed to achieve higher fuel flexibility and to improve emission performance [6]. Due to the high thermal inertia of the bed material, an even temperature distribution within the bed can be obtained. This makes it especially suitable for fuels with low calorific value, high ash content and high moisture content.

Mainly there exists two types of fluidized bed combustors, namely the bubbling fluidized bed (BFB) and the circulating fluidized bed (CFB), both of which are illustrated schematically in figure 2.1. The differences between the two types arises due to that they are operated at different fluidization velocities, BFB combustors are typically operated at 1-3 m/s whereas CFB combustors are typically operated at 3-6 m/s [7]. Owing to the higher fluidization velocities in CFB combustors, a large portion of the bed material becomes entrained with the gas flow in the boiler. Therefore, an external loop in which the entrained bed material is separated from the flue gases, by a cyclone separator, and recirculated to the bed is necessary. In BFB combustors the amount of entrained bed material is much less and thus the bed material separated in the cyclone is usually not fed back into the boiler. Furthermore, the BFB combustors has a well-defined bed surface while the solid concentration in CFB units decrease continuously with the height of the unit.

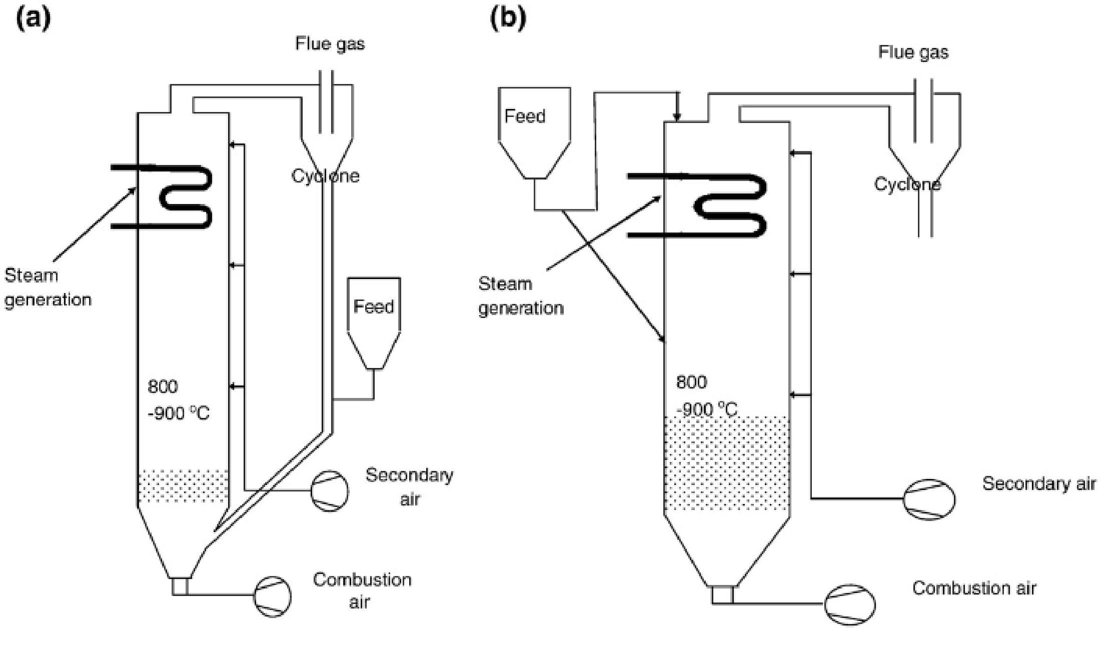

Figure 2.1: Schematic overviw of a CFB boiler (a) and a BFB boiler (b). [7]

In terms of sulphur removal, efficiency and scale, CFB boilers exhibits better performance than BFB boilers. However, BFB boilers handles variations in fuel moisture content better. This since the bed acts at heat buffers allowing higher heat transfer between particles. The ability to handle fuel moisture variations makes BFB boilers especially suitable for waste and biomass fuels, since these fuels are known to have wide variation of moisture content. Furthermore, the lower fluidization velocity and consequently longer residence times of bed material in BFB boilers, enables larger fuel particles and fuels with lower calorific value to be converted, compared to CFB boilers [6].

2.2 Conversion of solid fuels

Combustion of solid fuels is a complex process dependent on many parameters. The process may however be generalized into three reaction categories, namely fuel particle drying, solid particle pyrolysis and char oxidation [8]. The different categories occur during different instants of the combustion process. For large fuel particles, which is of interest for this work, the drying and the pyrolysis occur simultaneously in the initial stage of the combustion process. The char oxidation on the other hand commences after the first two reaction categories has occurred.

Both drying and pyrolysis are similar in that they both are processes driven by heat. During the drying, the fuel particle absorbs heat from the furnace environment and heats up. The moisture contained within the pore structure of the fuel is then evaporated, thus leading to a dry solid particle. The pyrolysis, also known as devolatilization, on the other hand is the thermal decomposition of the fuel particle. As the fuel particle is heated and reaches sufficiently high temperature, the volatile matter of the fuel is released. In general, it can be said that two products are formed during the pyrolysis reactions, namely volatiles and char. Although certain pyrolysis reactions are exothermic, the overall nature of the pyrolysis is endothermic meaning that heat must be supplied to maintain the reactions.

After the pyrolysis and drying, the char and volatiles undergo oxidation. Of the total heat generation more than 70% comes from the oxidation of the volatile matter [9]. The oxidation of volatile matter occurs in a diffusion flame located at the boundary between oxygen and unburned volatiles. Thus, the rate of combustion is usually determined by the oxygen and volatile diffusions at the location of the flame [10].

The oxidation of char occurs as a heterogeneous gas-solid reaction which at the temperatures in typical combustor exhibit rapid chemical kinetics. Therefore, the reactions are limited by the mass transfer of oxygen rather than by kinetics [8]. All oxygen that reaches the surface of the char particle will react and convert the fuel. In general, the combustion of the char can be described by the mechanisms presented in equations 2.1 and 2.2.

$$C + O_2 \rightarrow CO_2 \tag{2.1}$$

$$C + 0.5O_2 \rightarrow CO \tag{2.2}$$

An alternative to combustion of solid fuels is gasification, which is achieved by letting fuel react with a restricted amount of oxygen. Like the combustion process, the fuel first is subjected to drying and pyrolysis before further reactions take place. The gasification consists of a series of endothermic reactions, meaning that heat must be supplied in order to maintain the gasification. This heat is usually taken from the heat produced in combustion reactions. The gasification process produces a mixture of combustible gases through a number reactions. Four of the major reactions are water-gas reaction, Boudouard reaction, Shift Conversion and Methanation, which are presented in equations 2.3-2.6 respectively [10].

$$C + H_2O \rightarrow H_2 + CO \tag{2.3}$$

$$C + CO_2 \rightarrow 2CO \tag{2.4}$$

$$CO + H_2O \rightarrow CO_2 + H_2 \tag{2.5}$$

$$C + 2H_2 \rightarrow CH_4 \tag{2.6}$$

2.3 The novel concept

Chalmers have recently developed a fluidized bed technology which has shown itself to exhibit promising properties. The concept works by inserting a chamber into a fluidized bed reactor and in that way dividing the reactor into two zones[4], which in this work are referred to as the primary and the secondary chamber. The walls delimiting the two zones do not extend to the bottom of the reactor, but instead a slit is present at the bottom of the walls. By having this slit the two zones can communicate with each other i.e. an exchange of energy and mass is allowed. Furthermore, by introducing two reactor zones it enables the possibility of having different fluidization media in the two zones. The reactor, which is schematically illustrated in figure 2.2, could be operated with a pressure difference between the two reactor zones, thus giving rise to different bed heights in the two zones.

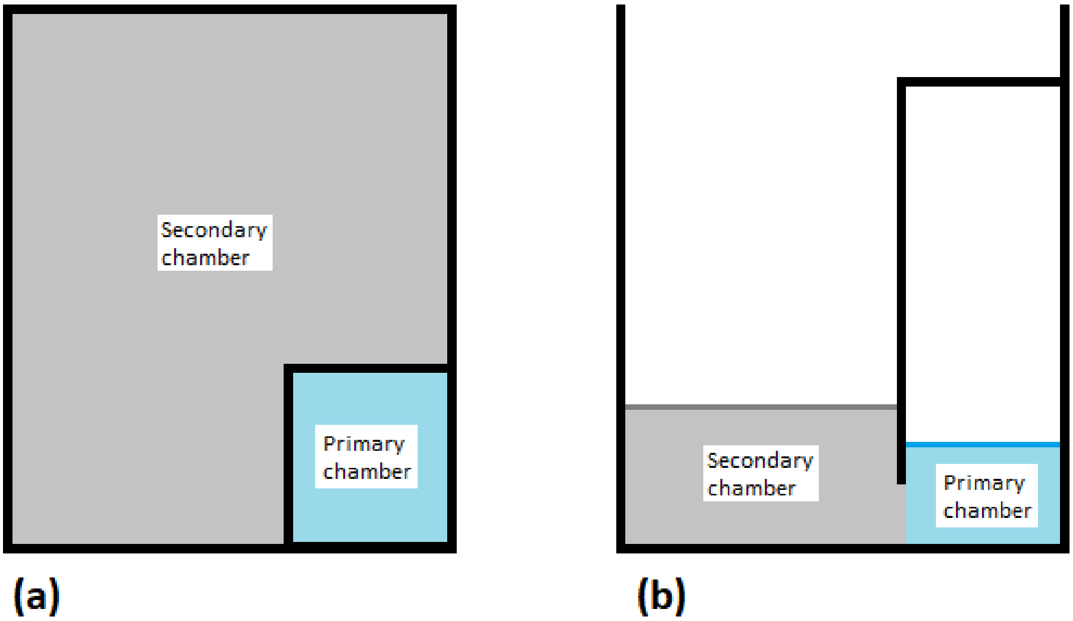

Figure 2.2: Schematic overview of the novel concept, (a) shows a view from above and (b) shows a view from the side.

Although different applications of the concept exist, the perhaps most interesting application is that of biomass combustion and gasification processes. In this application the presence of two communicating chambers would allow for drying and pyrolysis to occur in a different environment to char conversion. The biomass would be fed into the pressurized primary chamber, where drying and pyrolysis would occur. The remaining char fraction could then be transported out of the chamber to be converted. Given that the heat transfer between the two chambers is sufficiently good, the heat required for drying and pyrolysis could be supplied by the heat released during char conversion.

Several advantages could be achieved by performing the combustion or gasification process using the novel concept. From gasification perspective it would be advantageous due to reducing atmosphere produced during the release of volatile matter. The char gasification rate is highly decreased by the presence of a reducing atmosphere. Therefore, by separating the volatile matter flow from the char conversion region would increase the efficiency of the gasification [4]. Combustion processes could also be made more efficient by using the novel concept. In combustion the pyrolysis gives rise to regions close to the fuel feeding where the concentration of volatile matter is high. To avoid emissions of unburned volatile matter, higher excess air ratios would have to be used which in turn would have a negative effect on unit efficiency and capital cost.

Another advantage of the concept is that one could let the drying, pyrolysis and to some extent gasification occur in the primary chamber. In doing so the gas formed in this region could be extracted and later be used as either a source of energy or as precursor for biofuels or biochemicals [11] . Furthermore, the concept could be used to accommodate for changes in energy demand by controlling the process to produce different amounts of gas in the primary chamber. In periods of lower energy demand, more gas would be produced while less gas would be produced when the energy demand is higher.

For the concept to function effectively a number of criteria must be satisfied. Firstly, the mass transfer between the reaction zones should function as one-way valve in that fuel particles only should be transported out of the primary chamber. Secondly, the retention time of fuel particles in the chamber must be possible to control accurately. Thirdly, the gas environments of the two reaction zones should not be able to mix with each other. Lastly, compared to a conventional design, the implementation of the novel concept should not reduce the heat transfer between the zones too much so that temperature levels ensuring the good performance of both chambers are ensured.

2.4 Mixing in bubbling fluidized beds

Bubbling fluidized beds are characterized by the high degree of mixing they exhibit. Rowe et al. showed that the high degree of mixing mainly could be ascribed to the motion of bubbles through the bed [12]. Therefore, it is of great importance to understand the relation between bubble motion and solids mixing in the bed. By the means of experiments it has been determined that the solids mixing due to bubble motion can be described through three different mixing mechanisms. Firstly, the bubbles motion creates vortices at the trailing end of the bubble that bed solids are transported upwards by [13]. This region behind the bubble responsible for the upward motion of solids is often referred to as the wake of the bubble. Secondly a mechanism called drift which is due to the permanent displacement of solids outside the bubble. Thirdly, since solids are being transported upwards by the bubbles, a net downward flow of solids is induced at sides of the bubble to satisfy continuity.

The work presented in thesis is based on the assumption that mixing can be described as a two-phase system consisting of a bubble phase and an emulsion phase. In a bubbling fluidized bed, the bubbles introduce regions where the solids concentration is low. These regions are accounted for by the bubble phase. The emulsion phase on the other hand accounts for regions outside the bubbles where the solids concentration is higher. A schematic description of the model is presented in figure 2.3, where δ represents the bubble density which is defined as the volume fraction of the bed that is made up of bubbles.

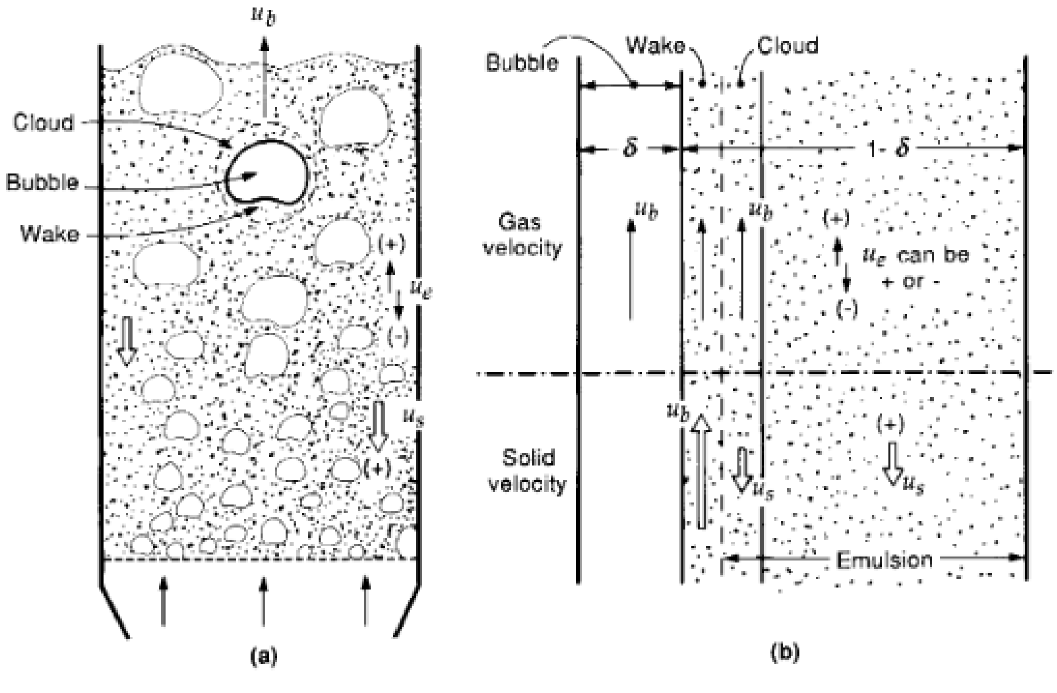

Figure 2.3: Schematic overview of the two-phase system, where (a) shows an actual dipiction of a fluidized bed and (b) illustrates how the two phases are defined.[17]

2.4.1 Bubble motion

There exist several empirical expressions that describe the velocity of a bubble in fluidized beds. One expression that is commonly used in literature for the rise velocity of a single bubble is that of Davidson and Harrison, which is presented in equation 2.7. In the expression u_{br} is the rise velocity of a single bubble, g is the acceleration due to gravity and d_b is the diameter of a spherical bubble with an equivalent volume to that of the spherical cap bubble [14].

$$u_{br} = 0.711\sqrt{gd_b} \tag{2.7}$$

As mentioned above, equation 2.7 expresses the rise velocity of a single bubble. However, in a bubbling bed bubbles coalesce when rising through the bed. The process of coalescence involves trailing bubbles accelerating into leading bubbles and therefore a higher average rise velocity is to be expected for the bubbles in a bubbling bed. In an attempt to account for bubbles traveling faster than the rise velocity of a single bubble, Davidson and Harrison proposed that all gas in excess of minimum fluidization (i.e. u_0 - u_{mf}) should contribute to the rise velocity, as presented equation 2.8 where u_0 is the fluidization velocity.

$$u_b = u_0 - u_{mf} + u_{br} \tag{2.8}$$

Experimental studies have however shown that expression presented in equation 2.8 tends to overestimate the rise velocity, since not all excess gas goes to the formation of bubbles. Instead it has been observed that there exist a throughflow of gas in and between bubbles. The expression for the rise velocity has thus been adjusted to account for the throughflow velocity (u_{tf}), yielding the expression presented in equation 2.9 [15].

$$u_b = u_0 - u_{mf} - u_{tf} + u_{br} \tag{2.9}$$

Based on research of Johnsson et al. [16] the throughflow velocity can be calculated according to equation 2.10, where z is the bed height, A_0 area of distributor plate per orifice and f_2 is factor that has been experimentally determined.

$$u_{tf} = (1 - f_2(z + 2.64\sqrt{A_0})^{0.4})(u_0 - u_{mf}) \tag{2.10}$$

f_2 can be calculated using equation 2.11 where d_p is the diameter of the bed solids.

$$f_2 = [0.26 + 0.70\exp(-3.3d_p)][0.15 + (u_0 - u_{mf})]^{-0.33} \tag{2.11}$$

Furthermore, the bubble density of the bubbling bed can be calculated through the expression presented in equation 2.12

$$\delta = \frac{1}{1 + \frac{1.3}{f_2}(u_0 - u_{mf})^{-0.8}} \tag{2.12}$$

2.4.2 Fuel motion in bubble phase

The description of the axial mixing in the bubble phase is derived from the empirical expressions for the bubble motion. The bed solids transported upwards in the bed via the wakes of the bubbles are assumed to travel at the same velocity as the bubbles. The amount of solids transported upwards in the wake is quantified by the wake fraction, which describes the ratio of the wake volume (V_w) to the bubble volume as presented in equation 2.13.

$$f_w = \frac{V_w}{V_b} \tag{2.13}$$

For irregular natural sand, experimental studies have shown that the wake fraction remains fairly constant independent on the diameter of the bed material. Typical values for the wake fraction of irregular sand lies within the interval of 0.2-0.3 [14].

Similar to the bed material in the bubble phase, the axial motion of the fuel particles is based on the bubble velocity. The fuel particles are assumed to travel in straight paths upwards in the bed at a fraction of the bubble velocity. The fuel particle velocity (u_f) can be calculated with equation 2.14, where alpha is an impact factor describing at what percentage of the bubble velocity the fuel particle is transported. The impact factor has in this work been set to a value of 0.3.

$$u_f = \alpha u_b \tag{2.14}$$

2.4.3 Fuel motion in emulsion phase

An expression for the velocity of bed solids in the emulsion phase can be derived by setting up a mass balance for the bed material. Given that bed material rises in the wakes of the bubbles, a downward flow of bed material must exist in order to satisfy continuity. A mass balance for the bed material is presented below in equation 2.15.

$$f_w \delta u_b + u_{sd}(1 - \delta - f_w \delta) = 0 \tag{2.15}$$

By rearranging the expression above, an equation for the velocity of the bed material in the emulsion phase (u_{sd}) can be formulated [17].

$$u_{sd} = -\frac{f_w \delta u_b}{1 - \delta - f_w \delta} \tag{2.16}$$

The motion of fuel particles in the emulsion phase can be calculated by setting up a force balance over a single fuel particle. The average fuel particle velocity is then assumed to equal the velocity yielding a zero net force on the fuel particle. The forces included in the force balance, which is shown in equation 2.17 are the gravitational force(F_G), the buoyancy force(F_B) and the drag force(F_D).

$$F_G + F_B + F_D = 0 \tag{2.17}$$

The gravitational force can mathematically be described as shown in equation 2.18, where m_f represents the mass of the fuel particle. The gravitational force is defined to be negative since the force is acting in a downward direction in the bed.

$$F_G = -m_f g \tag{2.18}$$

The buoyancy force is a function of the ratio between the density of the emulsion(ρ_e) and the density of the fuel particle(ρ_f) and can be expressed as shown in equation 2.19.

$$F_B = \frac{\rho_e}{\rho_f} m_f g \tag{2.19}$$

In contrast to the gravitational and buoyancy forces, which are constant forces only dependent on the inherent properties of the fuel particles and the bed material, the drag force is a function of the velocity of bed material in the emulsion phase. Therefore, the process of finding the fuel particle velocity becomes a question of finding the velocity that makes drag force equal the sum of the gravitational and the buoyancy forces. Depending on the relative sizes of the different forces in the force balance, the fuel particle velocity can be either positive or negative.

The drag force can be expressed as is illustrated in equation 2.20, where d_f is the fuel particle diameter, u_{rel} the relative velocity between the fuel particle and the bed material in the emulsion phase and C_D is the drag coefficient.

$$F_D = \frac{1}{2} \rho_e \frac{d_f^2 \pi}{4} C_D |u_{rel}| (u_{rel}) \tag{2.20}$$

In order to determine the size of the drag force, the drag coefficient must be known. Through experimental work, it has been determined that the drag coefficient can be related to the relative velocity according to the expression, presented in equation 2.21, where a and b be have been determined to be 0.48 and 1.3 respectively [15].

$$C_D = \frac{a}{u_{rel}^b} \tag{2.21}$$

2.4.4 Formation of endogenous bubbles

During drying and pyrolysis, a large amount of gas emitted from the fuel particles. It has been shown that this gas-emission can influence the nature of the fuel mixing in fluidized beds, as the emission induces a segregation effect on the fuel particles. The effect is so great that it alone can cause fuel particle segregation to the bed surface under circumstances that otherwise would ensure uniform mixing [18].

The segregation effect is caused by the emitted gas, which forms an endogenous bubble around the fuel particle. As the bubble is formed, the fuel particle falls down towards the trailing boundary of the bubble where it comes into contact with the emulsion phase. At this instance the motion of the fuel particle is dependent on an equilibrium between the drag and buoyancy of the rising emulsion phase behind the bubble, and the weight and inertia of the particle [19].

Depending on the relative size of the different contributions in the equilibrium, two different mechanisms of segregation can be observed. Firstly, if the drag and buoyancy initially is big enough to overcome the weight and inertia, a single bubble will cause the fuel particle to rise to the bed surface. This regime is referred to as single-bubble segregation (SBS). Secondly, if the bubble initially formed does not exert enough force on the fuel particle to make it rise to the bed surface, then the fuel particle uprise will occur stepwise. This regime is referred to as multiple-bubble segregation (MBS) and is characterized by the endogenous bubbles escaping from the fuel particle. For every escaping bubble, the formation of a new endogenous bubble is set off. The procedure of the bubble escaping and a new bubble forming will repeat itself until the drag and buoyancy overcomes the weight and inertia, thus giving rise to a stepwise uprise.

An expression for the extra lift force on a fuel particle undergoing drying and pyrolysis has been determined experimentally by Solimene et al. [18]. The expression is presented in equation 2.22, where Q represents the volumetric flow rate of the gas emitted from the fuel particle.

$$F_{lift} = 0.372 g^{\frac{3}{5}} \rho_e d_f Q^{0.8} \tag{2.22}$$

3

Modeling

3.1 Modeling

In general there exists two main tracks in modeling of fluid dynamics for fluidized bed combustors; macroscopic models that are based on empirical and semi-empirical expression and computational fluid dynamics (CFD) in which the fluid dynamics are described from first principle [20]. In a long term perspective the CFD-approach will likely become the preferred alternative for modeling. However, due to the long calculation times which for the time being is required for reliable results, CFD is not fully mature to replace macroscopic modeling altogether. In the void of technological advancements in the field of CFD, macroscopic modeling plays a crucial role and will probably do so for the foreseeable future.

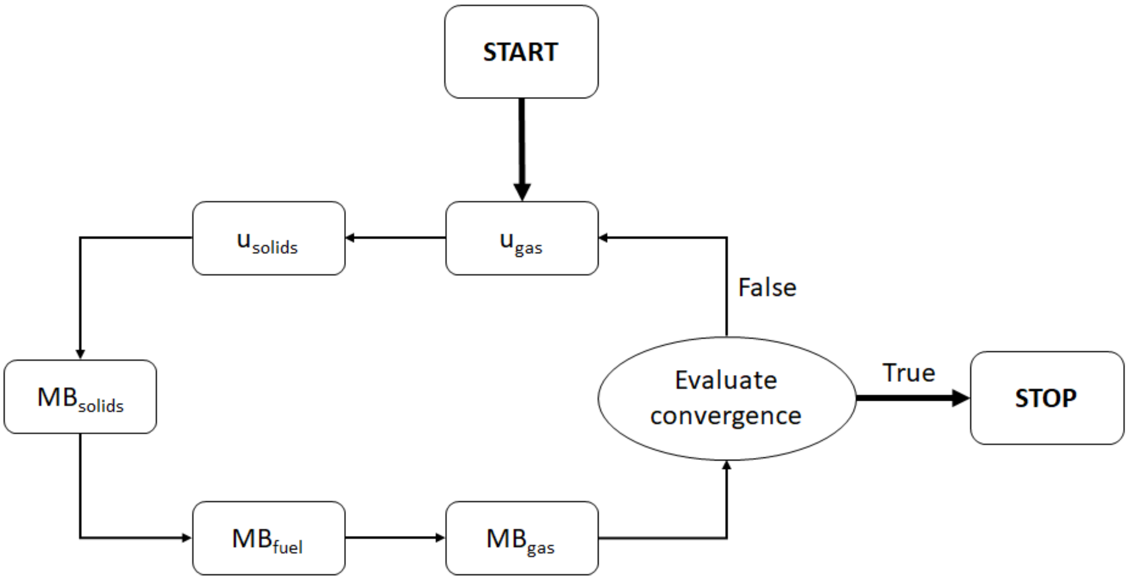

Figure 3.1: Schematic overview of the overall model structure.

The work presented in this thesis aim to describe the development of description of the axial mixing of biomass in fluidized bed combustors. This description is implemented into an already existing semi-empirical three-dimensional mathematical model that has been developed at Chalmers during the last decade. The overall structure of the model is illustrated in figure 3.1.

The model in turn and order solves equations for the gas velocity field, the solids velocity, the mass balance of solids, the mass balance of fuel and finally the mass balance of gases. After the equations have been solved, the convergence is evaluated based on two criteria. Firstly, by setting up a total mass balance and evaluating the total mass balance error. Secondly, the change in gas concentration fields for the present and the previous iteration is compared. The iteration loop is repeated until both the total mass balance error and the change in gas concentration falls below specified tolerance levels. In addition to the iteration procedure presented above, a heat balance can be solved in the model. However, the solving of a heat balance is beyond the scope of the work presented in the thesis. Therefore, description of the modeling for the heat balance has been omitted from this thesis.

3.2 Finite volume method

The governing equations describing the fluid dynamics of the fluidized bed are solved by implementing the finite volume method. The method works by dividing the geometry of interest into a number of control volumes, often referred to as cells. The division of the geometry into cells is illustrated in figure 3.1(a) and furthermore, a schematic representation of a single control volume is displayed in figure 3.1(b).

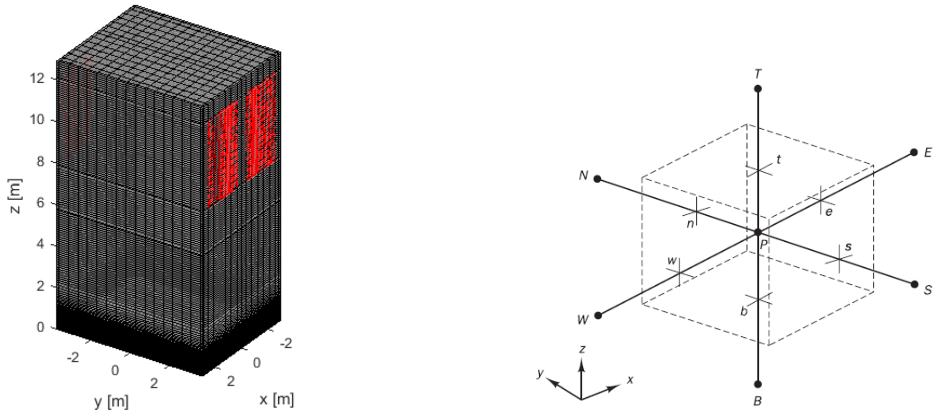

(a) **(b)**

Figure 3.2: Picture showing how a geometry has been divided into computational cells (a), and a picture illustrating a single computational cell (b).

In figure 3.1(b), the point P represents the node of the cell, which is the point at which the governing equations are solved for. The letters e, w, n, s , t and b stands for the direction relative to the cells, that is east, west, north, south, top and bottom. The upper case letters corresponds to the nodal points of the adjacent cell in the direction specified by the letter. The lower case letters corresponds to the points lying on the cells faces.

The transport equation for a convection-diffusion problem can be expressed in a general form as is presented in equation 3.1, where ϕ is quantity solved for, Γ is the diffusional coefficient and S_ϕ is the source term representing the net generation of quantity ϕ [21].

$$\frac{\partial \phi}{\partial t} + \nabla \cdot (\rho \phi \boldsymbol{u}) = \nabla \cdot (\Gamma(\nabla \phi)) + S_\phi \tag{3.1}$$

Fundamentally, the finite volume method works by integrating the differential equation to be solved over the control volumes making up the geometry. By doing this the expression presented in equation 3.2 can be obtained.

$$\int_{c.v} \frac{\partial \phi}{\partial t} dV + \int_{c.v} \nabla \cdot (\rho \phi \boldsymbol{u}) dV = \int_{c.v} \nabla \cdot (\Gamma(\nabla(\phi)) dV + \int_{c.v} S_\phi dV \tag{3.2}$$

The above expression can then be re-expressed using Gauss's divergence theorem, which is presented in equation 3.3.

$$\int_{c.v} \nabla \cdot (\boldsymbol{a}) \; dV = \int_A \boldsymbol{n} \cdot \boldsymbol{a} \; dA \tag{3.3}$$

The interpretation of Gauss's divergence theorem is that the integral of the divergence of a vector (a) can be expressed as flux of the vector field across the control volume boundaries. By applying Gauss's divergence theorem the version of the transport equation presented in equation 3.4 can be obtained. It should be noted that the accumulation term has been omitted from equation 3.4 since the equations solved in the model are stationary. Had the problem been time-dependent an integration with respect to time would also have to be made [21].

$$\int_A \boldsymbol{n} \cdot (\rho \phi \boldsymbol{u}) \; dA = \int_{c.v} \boldsymbol{n} \cdot (\Gamma(\nabla(\phi)) \; dA + \int_{c.v} S_\phi \; dV \tag{3.4}$$

Explicitly, equation 3.4 can be expressed as presented below in equation 3.5, where the source term has been approximated in a linear form. For the sake of simplicity a one-dimensional problem is considered in equation 3.5.

$$(\rho \boldsymbol{u} A \phi)_e - (\rho \boldsymbol{u} A \phi)_e = \left(\Gamma A \frac{d\phi}{dx}\right)_e - \left(\Gamma A \frac{d\phi}{dx}\right)_w + (S_u + S_p \phi_p) \tag{3.5}$$

When solving differential equations using the finite volume method, the fluxes through the cell faces must be evaluated. To evaluate the diffusional flux across the cell faces, both the gradient of ϕ and the diffusional coefficient must be approximated at cell faces. In the model this is done by implementing the upwind differencing scheme. One advantage of this scheme is that it takes into account the flow direction, by asserting that the face value can be approximated to equal the nodal value upstream to the flow direction [21]. The upwind differencing scheme thus yields the discretized form of the transport equation presented in equation 3.6, assuming flow in the positive direction.

$$F_e\phi_P - F_w\phi_W = D_e(\phi_E - \phi_P) - D_w(\phi_P - \phi_W) + S_u + S_p\phi \tag{3.6}$$

In the equation above F and D represents the quantities presented below in equations 3.7 and 3.8.

$$F = \rho u \tag{3.7}$$

$$D = \frac{\Gamma}{dx} \tag{3.8}$$

By rearranging the equations the form of the discretized equation presented in equation 3.9 can be obtained, where a_P is calculated as illustrated in equation 3.10

$$a_P\phi_P = a_W\phi_W + a_E\phi_E + S_u \tag{3.9}$$

$$a_P = a_W + a_E + (F_e - F_w) - S_p \tag{3.10}$$

Using the discretized equations above, the problem of solving the governing equation becomes a matter of determining numerical values of the a-coefficients and the source terms. Using the upwind differencing scheme, the a-coefficients for a one-dimensional case can be calculated as presented in table 3.1.

Table 3.1: Table showing how a-coefficient is calculated for a one-dimensional problem

a_W	a_E
$D_w + max(F_w, 0)$	$D_e + max(0, -F_e)$

The same discretization procedure as is presented above, can be applied to three-dimensional problem, yielding a similar form which can be expressed as seen in equation 3.11, where the index n.b stands for neighboring cells.

$$a_P\phi_P = \sum_{n.b} a_{n.b}\phi_{n.b} + S_u \tag{3.11}$$

Similarly, the a_p coefficient can be expressed as shown below in equation 3.12, where dF is the net convection into the control volume of interest.

$$a_P = \sum_{n.b} a_{n.b} + dF + S_p \tag{3.12}$$

3.3 Mass transfer between phases

Essential for the two-phase modeling approach is to determine the mass transfer between the bubble and emulsion phase. Since all fuel is fed into the emulsion phase, the only way that fuel can enter the bubble phase is through mass transfer from the emulsion phase. The size of the mass transfer between the phases has been investigated using magnetic particle tracking (MPT) in a down-scaled laboratory unit [15]. By tracking the motion of magnetic tracer with properties resembling that of typical biomass fuel particle, the probability of mass transfer to the bubble phase for different heights in a fluidized bed could be determined. Measurement data for the probability (q_z) in fluidized bed with an up-scaled bed height of 30 cm is presented in figure 3.3. It should be noted that the probability of mass transfer differs slightly depending on the properties of the fuel and the bed.

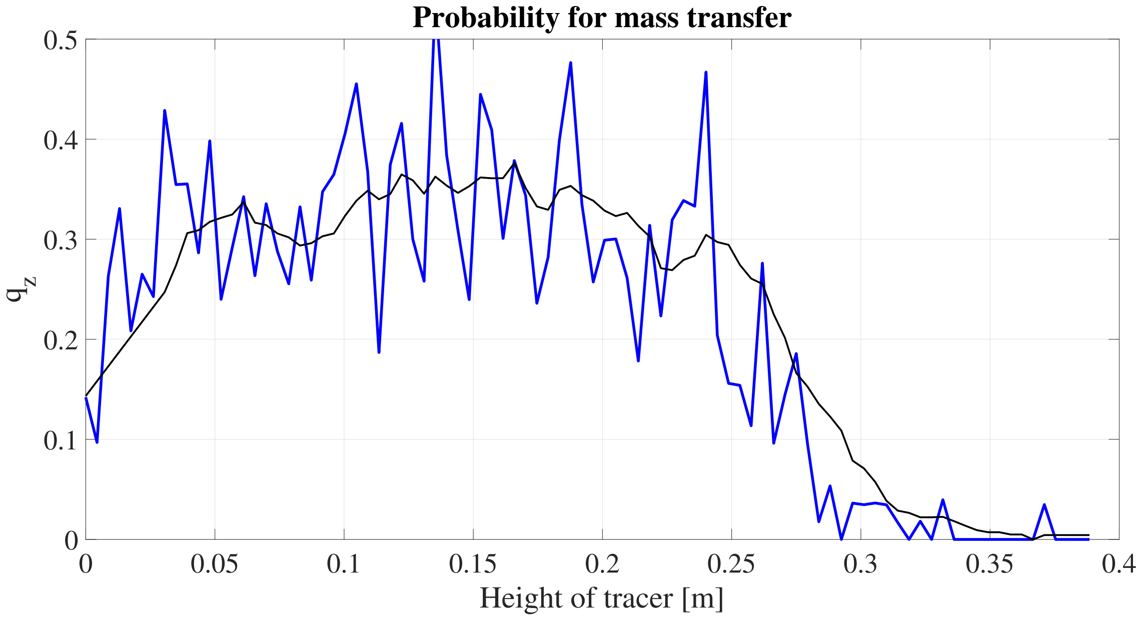

Figure 3.3: Experimental data from MPT-experiments relating the height in the bed to the probability of mass transfer from the emulsion phase to the bubble phase.

For a large portion of the bed, the probability remains fairly constant at a value of approximately 0.3. Therefore, the probability of mass transfer is set to 0.3 for all heights of the bed. From a phenomenological perspective the fuel particle uprise, and consequently also the mass transfer to the bubble phase, is set off by the bubbles rising in the dense bed. Therefore, the mass transfer from emulsion to the bubble phase must be related to the bubble frequency in the bed. The size of the mass transfer contribution, which is set as a negative source term in the emulsion phase and a positive source term in the bubble phase, can thus be quantified by the expression presented in equation 3.13.

$$S_p = q_z f_{bub} c_{fuel} V \tag{3.13}$$

In the equation c_{fuel} represents the fuel concentration in the cell, V the volume of the cell and f_{bub} the bubble frequency in the bed. The bubble frequency can be quantified using the expression presented in equation 3.14, which was derived by Baskakov et al. [22].

$$f_{bub} = \frac{1}{\pi}\sqrt{\frac{g}{z}} \tag{3.14}$$

In the two-phase model there also exists a mass transfer in the opposite direction i.e. from the bubble phase to the emulsion phase. This mass transfer takes place as the fuel reaches the bed surface. The size of this mass transfer is equal to the convective flux that would have been transported through top faces of the mesh layer located at the bed surface. In the bubble phase negative source terms are introduced at the bed surface whereas equal but positive source term are introduced in the emulsion phase. The size of the source term can be expressed as presented in equation 3.15, where u_t is the axial fuel velocity in the top layer and A_t is the cell area of the top face.

$$S_p = -c_{fuel} u_t A_t \tag{3.15}$$

3.4 Classes

Both combustion and gasification of solid fuels is characterized by the coexistence of fuel particle of different sizes and densities. The fuel fed into the boiler is not of uniform size and furthermore as the fuel particles undergo reactions it brings about changes in both density and particle size. In the model this distribution of fuel particle properties is accounted for by the introduction of classes, where each class represents fuel particles of a certain size and density. For each of the defined classes the transport equation is solved, and different behavior for fuel particles of different sizes can thus be accounted for.

In the model there are two types of classes namely, size classes and conversion classes. The size classes are used to capture the polydispersity of the fuel fed into the boiler by specifying a series of initial fuel sizes. For each of the different size classes, a number of conversion classes are specified to model the change in size and density due to reactions. As is illustrated in figure 3.4, the first step is that the transport equation for the first conversion class is solved. When doing so, source terms are introduced in the second conversion class. In the same way the transport equation for the second conversion class is then solved, and source terms are introduced in the following conversion class. This procedure is repeated until transport equations for all pre-defined conversion classes have been solved.

The conversion classes can be subdivided into two categories, where the first category is drying and devolatilization classes. These classes represent the initial stages of

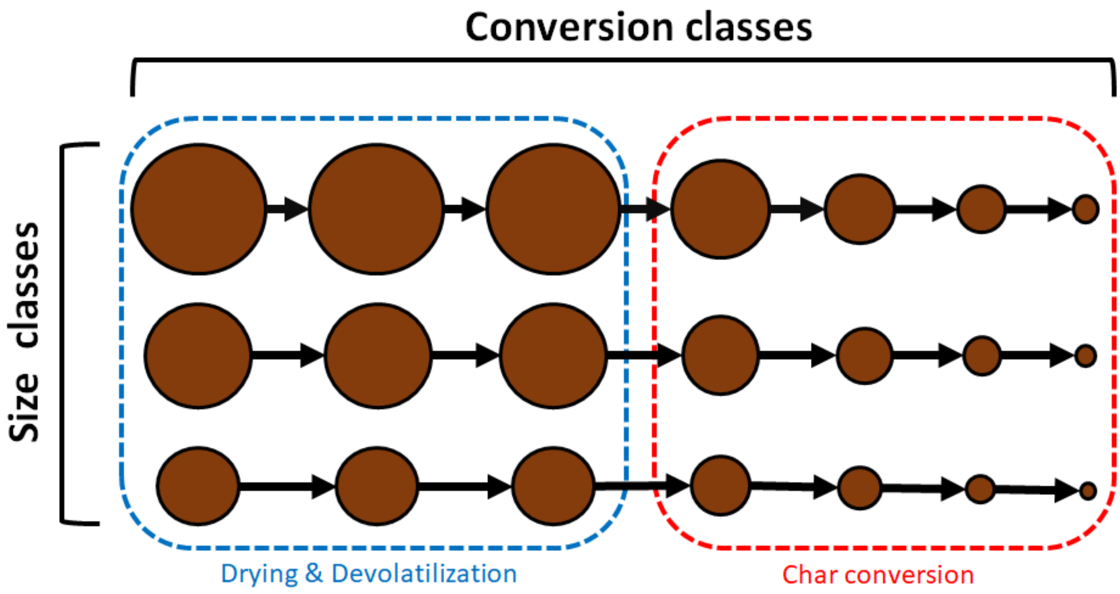

Figure 3.4: Schematic overview of the concept of classes

the solid fuel conversion where drying and pyrolysis occurs. In the model it is assumed that the diameter of the fuel particle remains constant during the drying and devolatilization classes and that instead the density decreases.

Following the drying and devolatilization classes, a number of char conversion classes are specified where the char fraction of the solid fuel is converted either through combustion or through gasification. Comparing the diffusion rate of O_2 into the fuel particle to the rate of char conversion, it can be concluded that the conversion rate is higher than the diffusion rate of O_2. Therefore, it can be assumed that the reactions will take place close to the surface of the fuel particle and that the fuel can be considered to be in the shrinking sphere regime [23]. Consequently, when modeling the char conversion classes, the density is kept at a constant value while the diameter of the fuel particle decreases.

3.5 Modeling of chemistry

The first steps that occur during the conversion of solid fuel drying and pyrolysis. In the model these processes are assumed to occur simultaneously and that a time for volatile matter to be released can be specified. It is possible to model the time for volatile release, but for the work presented in this thesis the time has been set to a constant value of 20 s corresponding to a typical pyrolysis time. The pyrolysis time is divided in to equal parts, so that the pyrolysis time for all of the individual conversion classes is equally large.

Combustion and gasification processes are also accounted for in the model by including a number of reaction mechanisms. These reactions can be divided into heterogeneous and homogeneous reactions. For heterogeneous reactions the species consumed are in different phases, i.e gas phase and solid phase. The rate of reaction, both for heterogeneous and homogeneous reactions, are determined through the Arrhenius equation which is commonly used to model the how the reaction rate depends on temperature [24]. The Arrhenius equation is as stated below in equation. 3.16.

$$k = A \exp\left(\frac{-E_A}{RT}\right) \tag{3.16}$$

As can be seen in the Arrhenius equation, the rate of reaction (k) is dependent on a pre-exponential factor (A), the activation energy(E_A) and the temperature (T) at which the reaction occurs. The heterogeneous reactions that are accounted for in the model are presented in table 3.2 along with values for pre-exponential factor and activation energies used in the model.

Table 3.2: Table showing reaction mechanisms for heterogeneous reactions

	Reaction	$E_0[\frac{J}{mol}]$	A
1	$C + O_2 \rightarrow CO_2$	75 000	3 160
2	$C + 0.5O_2 \rightarrow CO$	75 000	4 470
3	$C + H_2O \rightarrow CO + H_2$	75 000	600
4	$C + CO_2 \rightarrow 2CO_2$	75 000	600

Of the reactions presented above in table 3.2, the first two reactions represent char combustion, whereas the last two reactions represent char gasification. It is cumbersome to determine the exact rate of reactions for solid fuel conversion, however it is known that the combustion rates are faster than the gasification rate. Therefore, the rate of reaction for the combustion reactions in the model has been set to be approximately five times greater than the gasification rate of reaction. This is achieved by setting the activation energy for all reactions to the same value and specifying pre-exponential factors to be five times greater for the combustion reactions, compared to the gasification reactions. Furthermore, since no heat balance is solved in the current version of the model, a uniform temperature of 850 $°C$ has been set for all locations in the boiler.

The homogeneous reactions, which are reactions where all reacting species are in the gas phase, that are accounted for by the model are presented in table 3.3. The values for activation energies and pre-exponential factors are taken from experimental investigation studies for gasification of sewage sludge [25].

Table 3.3: Table showing reaction mechanisms for homogeneous reactions

	Reaction	$E_0[\frac{J}{mol}]$	A
1	$H_2 + 0.5O_2 \rightarrow H_2O$	$10.8 \cdot 10^6$	125 525
2	$CO + 0.5O_2 \rightarrow CO_2$	$130 \cdot 10^6$	26 225
3	$CO + H_2O \rightarrow H_2 + CO_2$	0.2778	12 560
4	$H_2 + CO_2 \rightarrow CO + H_2O$	3.289	34 730

3.6 Governing equations

As mentioned earlier, the model runs through an iteration procedure where it solves a number of governing equations. The first equation solved is a potential flow function for the gases. The equation reads as presented in equation 3.17

$$0 = D\nabla^2\psi + n''' \tag{3.17}$$

where D is an arbitraty diffusion coefficient, n''' is gas generation from non-equimolar reactions and ψ is the potential function for the gas velocity. Once the potential function has been solved for, the gas velocity can be calculated as presented below in equation 3.18, where p is the pressure.

$$\boldsymbol{u_g} = \frac{RT}{p}(D\nabla\psi) \tag{3.18}$$

Similarly to the gas flow, the solids velocity is solved through a potential flow equation, which is presented in equation 3.19.

$$0 = D\nabla^2\psi \tag{3.19}$$

The velocity of the solids are the solved through the equation 3.20

$$\boldsymbol{u_s} = D\nabla\psi \tag{3.20}$$

Once the velocities for the gas flow and the solids flow has been calcluated, a mass balance for the solid material is solved. The mass balance for the solids can be expressed as shown in equation 3.21 where $\dot{m}'''$ is the net generation of solids from other solids classes.

$$\nabla \cdot (c_s\boldsymbol{u_s}) = D\nabla^2 c_s + \dot{m}''' \tag{3.21}$$

Following the solids mass balance, a mass balance for the fuel is solved. This equation has the same form as the mass balance for the bed solids, with the difference that the net generation arises from other fuel classes. The equation is presented below in equation 3.22.

$$\nabla \cdot (c_f\boldsymbol{u_f}) = D\nabla^2 c_f + \dot{m}''' \tag{3.22}$$

Finally, a mass balance for the gas species in the system is solved. This mass balance is shown below in equation 3.23 where w_i is the volume concentration of gas species i and n''' is the net generation of gas species.

$$\nabla \cdot (\rho\boldsymbol{u_g}w_i) = D\nabla^2\rho w_i + n''' \tag{3.23}$$

3.7 Fuel mass balance algorithm

The description of the axial fuel mixing developed in this thesis, is implemented into the existing mathematical model by introducing a new algorithm for the fuel mass balance. The aim of the algorithm is to find a-coefficients and the source terms needed to solve the system of equations describing the mixing. The algorithm used to calculate the a-coefficients and source terms is schematically presented in figure 3.5.

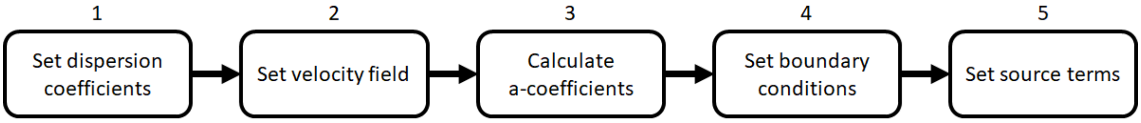

Figure 3.5: Schematic overview of the algorithm for calculating a-coefficients and source terms.

The first step of the algorithm is to specify dispersion coefficients, which is of special importance since it offers a way of describing the lateral mixing in the bed. Following the first step, the velocity field of the fuel is specified. This is done in accordance with the procedure presented in section 2.4.

Once the velocity field has been calculated and specified the three remaining steps in the algorithm are the calculation of the a-coefficients, the specification the boundary conditions and finally the specification of the source terms. In the model, the concentration fields of the bubble and the emulsion phase are solved simultaneously. This is done by first performing steps 1-5 in figure 3.5 for the emulsion phase and then repeating steps 1-5 but for the bubble phase instead. The a-coefficients and the source terms obtained can then be used to formulate the system of equations in a sparse matrix form.

To obtain the concentration fields for the fuel, both in the emulsion and in the bubble phase, the system of equations is solved. This done by using the MATLAB-function bicgstabl, which solves a system of equations of the form $Ax = b$ with the biconjugate gradients stabilized method. In the model the matrix A represents the sparse matrix containing the a-coefficients, b a column vector containing the constant source terms and x is the vector representing the concentration values of the cells in the geometry.

4

Simulations

To evaluate the performance of the novel multi-staged fluidized bed concept a number of simulations has been performed. All of these simulations have been performed using identical geometries. The simulated unit, which can be seen schematically in figure 4.1 has width 5.9 m a depth of 7.4 m and height of 12.92 m. Furthermore, the primary chamber which is introduce into to unit is placed in the bottom right corner, relative to the picture, and has the dimensions of 3x2 m.

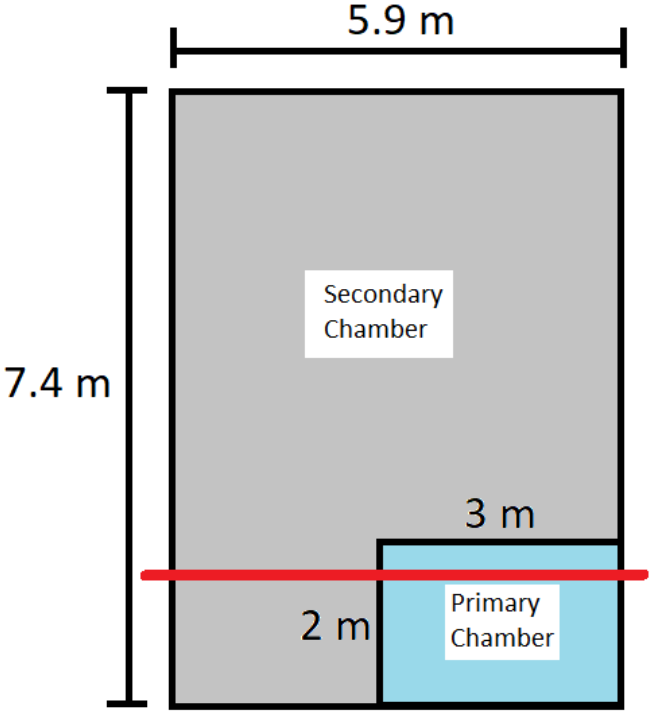

Figure 4.1: Geometry dimensions used for the simulations

For all simulations presented in the results, only one size class has been considered, meaning that all fuel particles will have an equal initial particle diameter. If nothing else is stated, the initial fuel particle diameter will be set to 2 cm. Furthermore, all fuel will be fed into the primary chamber to be able to observe the tendency for fuel to be transported out of the chamber. For all simulations, excluding the simulations investigating surface loading which will be discussed in section 4.1, the size of the fuel injection will be 1 kg/s. Other values variables that must be specified in the model is presented in Appendix A.

Three types of results are going to be presented in the report. The following sections will address how the different results was obtained

4.1 Concentration profiles of individual classes

As a part of the result presented in the thesis, fuel concentration profiles in the fluidized bed have been plotted. All concentration profiles will be presented along a cut-through of the fluidized bed unit. The position at which the concentration profiles are taken illustrated in figure 4.1 by the red line in the bottom of the picture and is located 1.77 m from the wall. Furthermore the concentration profile will only be plotted to the bed height, which for all simulations is 80 cm. All information above this height will be omitted from the figures.

As in the previous chapter, the mathematical model solves for concentration fields for each of the classes that are modeled. To observe possible difference in behavior between fuel particle undergoing drying and pyrolysis and char particles being converted, total concentration fields for the two types of conversion classes have been calculated. This is achieved by adding together all drying and devolatilization classes to one concentration field and to add all char conversion concentration fields together.

4.2 Surface loading

The surface loading β, that is to say the accumulation of fuel at bed surface, has been calculated for a number of simulations. This was done by calculating which percentage of the uppermost layer of the bed in the primary chamber consisted of fuel, according to equation 4.1.

$$\beta = \frac{[\text{Mass of fuel}]}{[\text{Mass of fuel}] + [\text{Mass of bed solids}]} \tag{4.1}$$

The surface loading has been calculated based on a number of different fuel feed rates, ranging from 0.2 kg/s to 2.5 kg/s. The feed rate has however been normalized against the cross-sectional area of the primary chamber as to enable the findings from the simulations to be utilized in a general case.

4.3 Sensitivity analysis

A sensitivity analysis was performed in order to determine how the novel concept is affected by changes in operation parameters. This was done by performing simulations with different values for three parameters. The three parameters investigated was the pressure difference between primary and secondary chamber (ΔP), height of the slit (h_{slit}) and the fluidization velocity (u_0). The metric used to determine how the performance of the novel concept changed was the amount of char gasification taking place within the primary chamber.

In addition to the amount of char gasification taking place in the primary chamber, the sensitivity analysis also offers an understanding of how much of the char fraction that is transported out of the primary chamber. All char that is not converted in the primary chamber is obviously transported out of the chamber in order to satisfy the mass balance.

5

Results and discussion

5.1 Concentration profiles of individual classes

To illustrate differences in behaviour between fuel particles in different stages of the conversion, concentration fields for the different fuel particle classes are plotted. In figure 5.1 the total concentration field for all drying and devolatilization classes is presented.

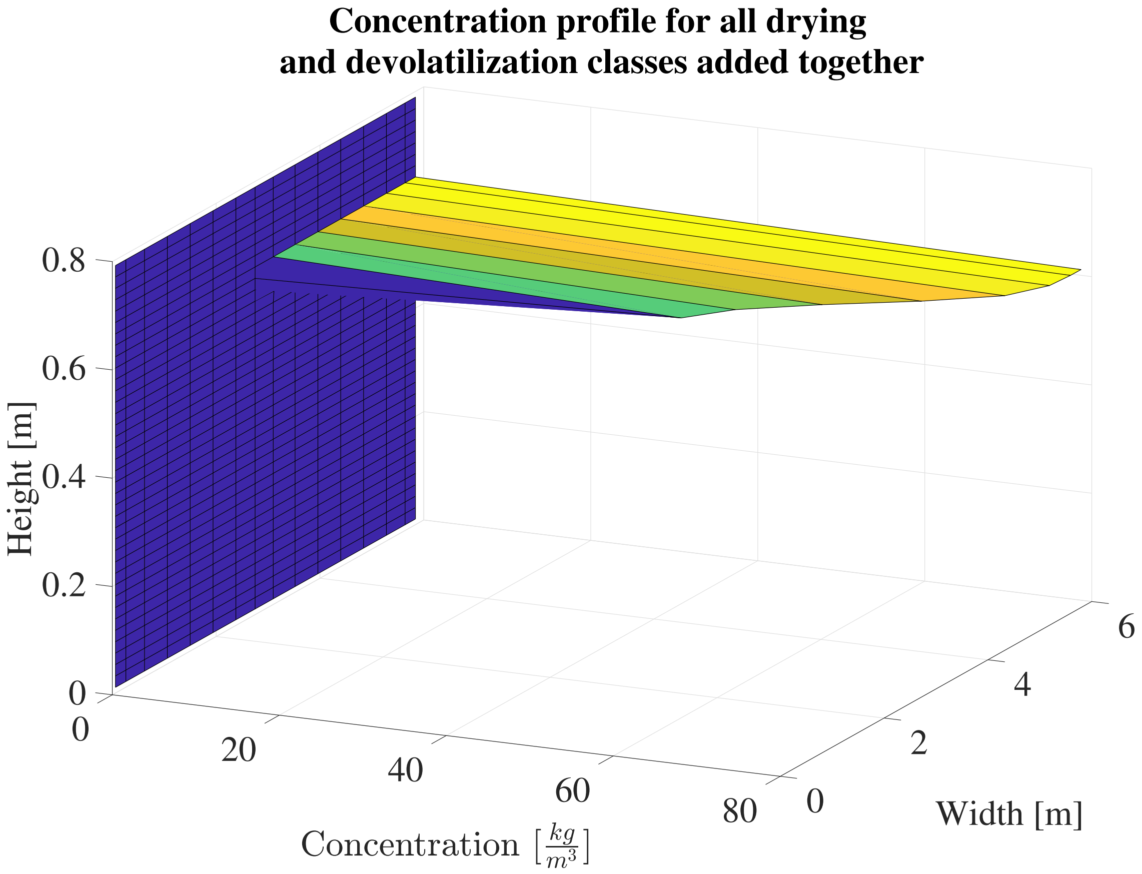

Figure 5.1: Total concentration profile for all drying an devolatillization classes.

Looking at figure 5.1 it can be seen that for the drying and devolatilization classes the concentration profile exhibits a strong concentration maximum at the bed surface of the primary chamber. The concentration reaches a value of about 80 kg/m^3 at the bed surface, whereas the concentration in the bed is virtually zero. Furthermore, the amount of fuel exiting the primary chamber is almost non-existent. This behaviour is to be expected for the drying and devolatilization classes. During these processes a large amount gas is emitted from the fuel particle and thus bringing about the formation of endogenous bubbles. The formation of endogenous bubbles gives rise to an additional lift force to the fuel particle force balance and in turn giving a higher upward velocity for the fuel particles.

From an operational perspective for the novel concept, the segregating tendency of the fuel particles is beneficiary since it to a greater extent allow for the drying and pyrolysis to occur within the primary chamber. However, questions could be raised to whether too much fuel accumulates at the bed surface and in that way resulting in fuel particles floating on top of the bed and not reacting. Given the large effect the formation of endogenous bubbles have on the mixing during drying and pyrolysis, further studies regarding the pyrolysis time would offer valuable information on the segregation behaviour.

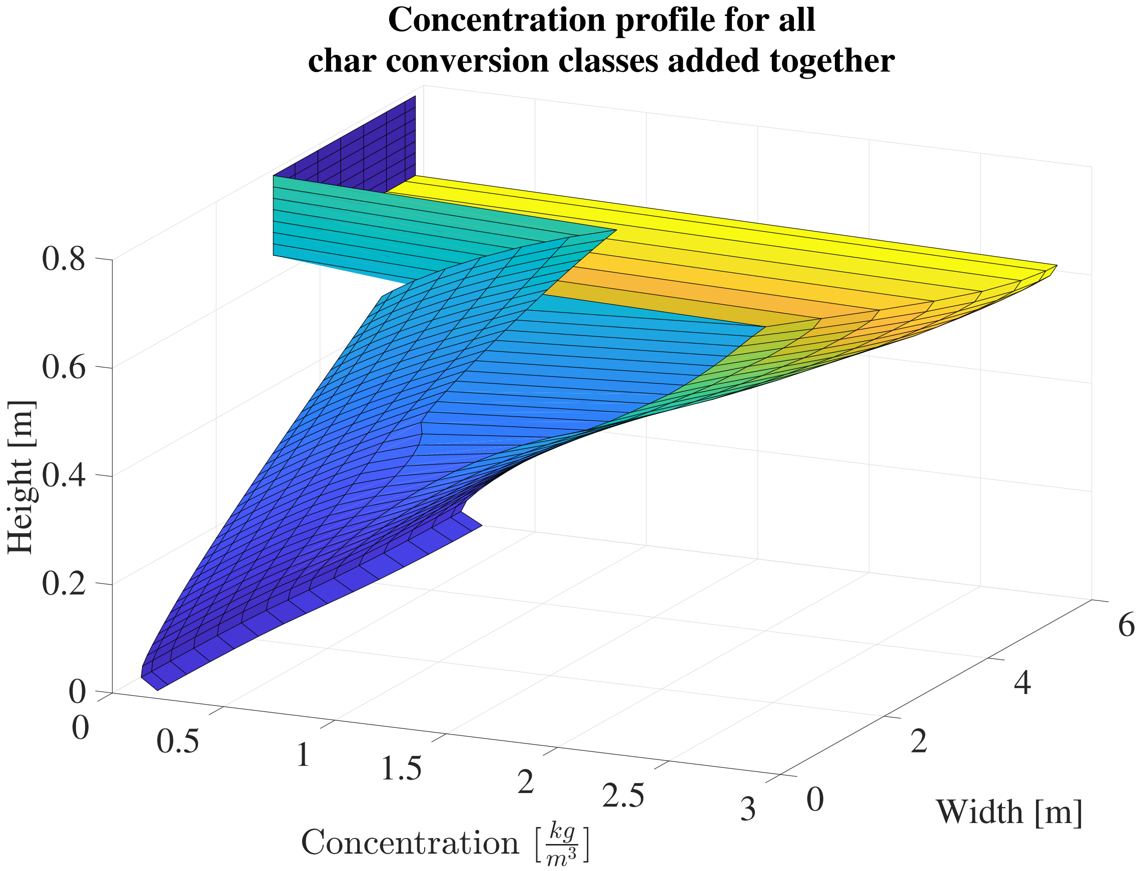

Figure 5.2: Total concentration profile for all char conversion classes.

The corresponding concentration profile, where all char conversion classes has been added together is presented in figure 5.2. Comparing 5.1 and 5.2 it can be seen that there are significant differences between the drying and devolatilization classes and the char conversion classes. The char conversion class concentration become more distributed through the bed and as a consequence the amount of fuel exiting primary chamber is noticeably higher. The observed trends seem reasonable given the assumption made in the model that endogenous bubbles does not form around char particles. Following from this is assumption, the upward force component in the fuel force balance will decrease compared to drying and devolatilization case. Furthermore, the char conversion is assumed to occur in the shrinking sphere regime, which leads to smaller fuel particles as the fuel progresses through the conversion classes. Since the buoyancy is exhibits a stronger dependency on the particle size as compared to drag force, the shrinking fuel particles will lead to increasing downward velocity of the fuel in the emulsion phase.

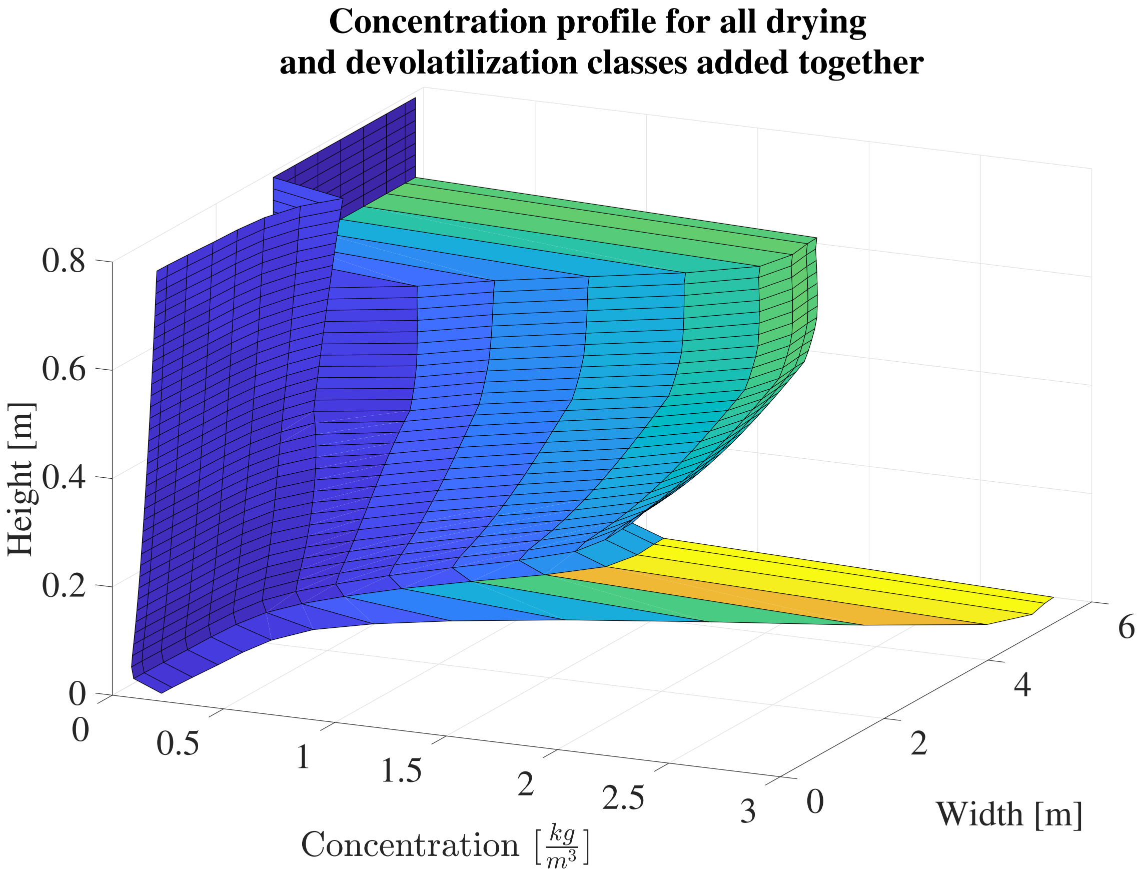

Figure 5.3: Total concentration profile for all drying and devolatilization classes for fuel particles with an inital diameter of 5mm.

Figure 5.3 displays a concentration profile for a case where the diameter of the fuel particle has been decreased to a size of 5 mm. As can be seen the behavior where the drying and devolatilization classes accumulates at the top of the fluidized bed is not achieved for this simulation. Instead the highest concentration is located in the bottom of the bed. The main effect causing the this trend is the large difference in the volumetric gas flow of emitted gas from the fuel particle during drying and pyrolysis. Owing to the assumption that the pyrolysis time is constant for all fuel sizes, the volumetric flow rate decreases dramatically for smaller fuel. In table 4.1 the volumetric flow rate emitted from particles in a single drying and devolatilization class, for a series of different particle sizes is presented.

Table 5.1: Table displaying volumetric gas flow emitted from fuel particles of different sizes.

$d_f[mm]$	20	15	10	5
$Q[m^3/s]$	$6.89 \cdot 10-4$	$2.91 \cdot 10^{-4}$	$8.61 \cdot 10^{-5}$	$1.08 \cdot 10^{-5}$

Looking at the relative sizes of the volumetric flows it can be seen that the volumetric flow for particles with a diameter of 20 mm is approximately 64 times greater than the volumetric flow rate observed for 5 mm case. Since the lift force due to endogeneous bubble formation is function of the volumetric flow of emitted gases, the observed trend is to be expected for smaller fuel particles. This fact further suggests that the correct determination of pyrolysis time is of great importance for the description of the fuel mixing behavior in fluidized bed.

5.2 Surface loading

The surface loading is plotted as a function of the normalized amount of fuel fed into the primary chamber in figure 5.4. As can be the surface loading increases as the amount of fuel fed into the chamber increases. Considering the behavior observed in the previous section 5.1, where the fuel concentration is significantly higher at the top of the bed compared to lower regions of the bed, the trend of increasing surface loading is expected. The amount of fuel fed into the primary chamber probably would not introduce any effects that would cause the trend with high concentrations close to the surface to be altered. Therefore, the higher concentrations associated with larger fuel feeds is expected to bring about higher values for the surface loading.

The fuel particle diameter could perhaps influence the relation between the amount of fed fuel and the surface loading. As was illustrated in the previous section, for fuel particle with a diameter of 5 mm the highest concentration was achieved at the bottom of the bed instead of at the surface. Therefore, it is not certain that increasing the fuel feed would increase the surface loading if the fuel particle is too small. The mixing behavior of small fuel particles could however be a consequence of the fact that the pyrolysis time is assumed constant.

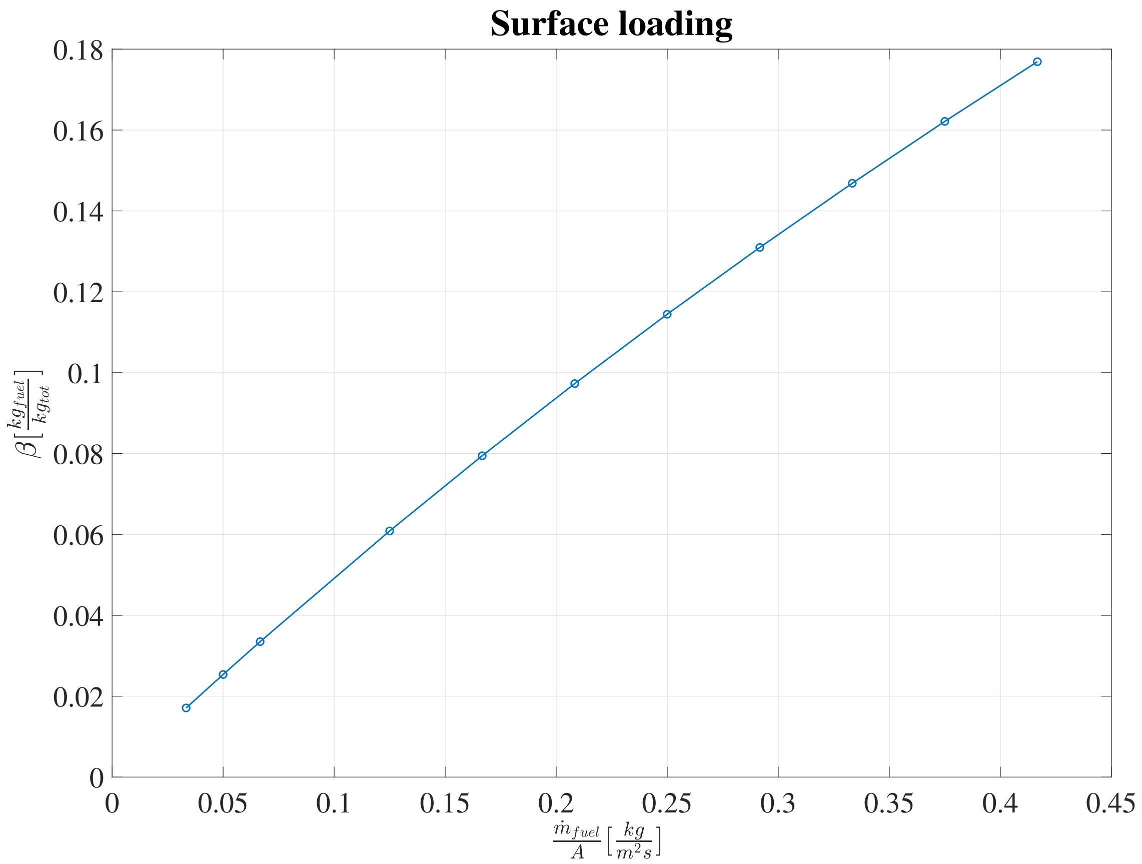

Figure 5.4: Surface loading for different fuel feed rate into primary chamber.

For combustion processes neither a too high or a too low surface loading is desirable from an operational perspective. Too high concentrations could lead to temperature locally could become so high that bed material may start to agglomerate. A too low temperature is not desirable since the efficiency of the combustor then could be decreased. For gasification processes however, it is uncertain how high or low surface loadings may affect the process. Perhaps a too high concentration could lead to too low temperature owing to the endothermic nature of the gasification process.

5.3 Sensitivity analysis

A sensitivity analysis was performed to determine how variations in operational parameters affects the performance of the novel fluidized bed concept in terms of the extent of char gasification occurring in the primary chamber. For the results presented in this section, three parameters were varied: the pressure difference between the two reaction zones, the fluidization velocity and the height of the slit under the delimiting walls. For all simulations one initial fuel size have been considered, that is a fuel diameter of 20 mm. The result of the sensitivity analysis is presented in figure 5.5.

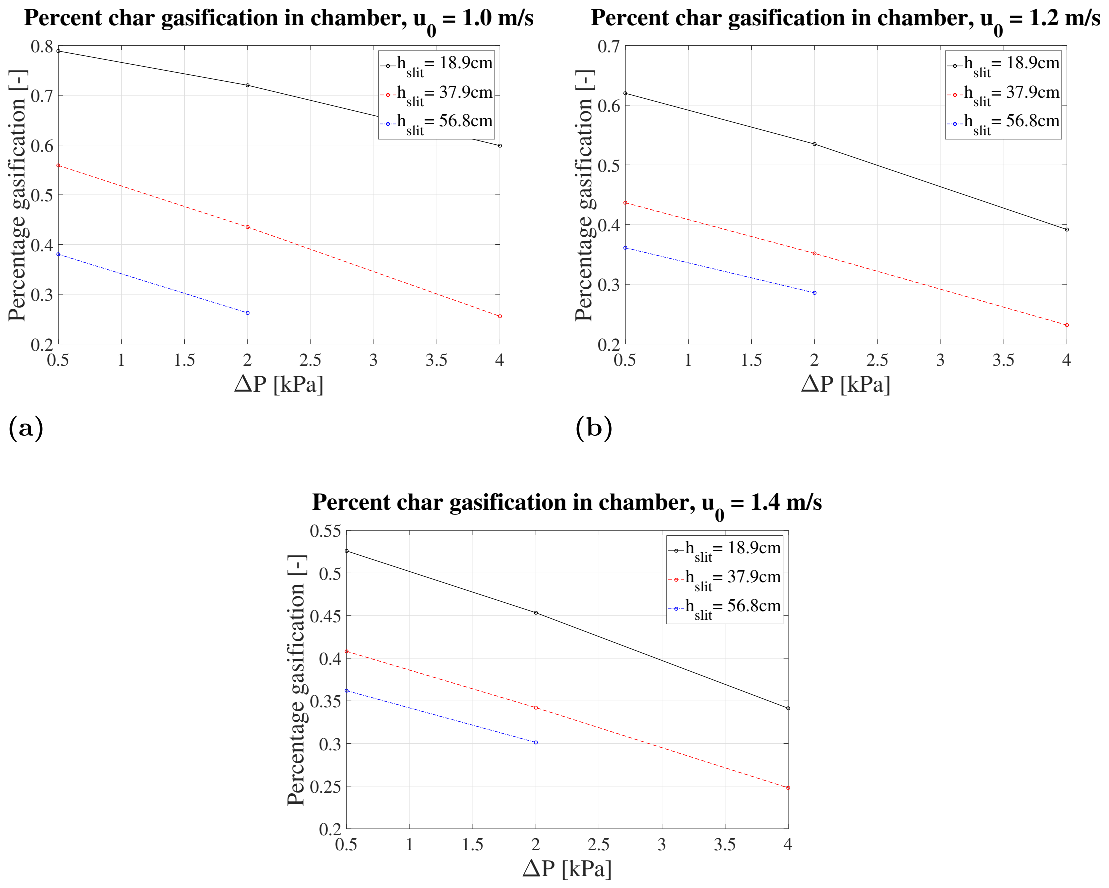

(a) (b) (c)

Figure 5.5: Sensitivity analysis where the extent of char gasification is related to ΔP, h_{slit} and u_0. Figures (a), (b) and (c) correspond to fluidization velocities of 1.0, 1.2 and 1.4 m/s respectively.

Comparing the amount of gasification for the different cases, a number of trends can be observed. Firstly, it can be seen that the amount of gasification decreases as the height of the slit is increased. This result is to be expected since a bigger slit height allows for a greater area at which material can exit the primary chamber. The slit height has a great effect on the amount of gasification occuring, much effort thus must be put on finding the optimal slit opening to install in a unit. It becomes especially important because it contrary to the pressure difference and the fluidization velocity cannot be used as a control parameter.

Looking at how the pressure difference affects the amount of char gasification it can be seen that an increase in pressure difference leads to a decrease in the amount of char gasification in the primary chamber. This is due to the fact that the pressure difference causes a lower bed height in the primary chamber and as consequence the bed surface location comes closer to the opening between the primary and secondary chamber. As the pressure differences is further reduced the bed height in the primary chamber also decreases and thus explaining the trend of decreasing amount of char gasification. Since changing the pressure difference gives rise to significant differences in amount of char gasification, the pressure difference could be used as an control parameter to control the retention time in the primary chamber.

The amount of char gasification can also be decreased by increasing the fluidization velocity. This can be understood by the higher degree of mixing induced as the velocity is increased. Increasing the fluidization velocity results in a greater bubble velocity upwards in the bed and consequently also a higher velocity for the solids travelling in the wake of the bubbles. Therfore to satisfy continuity, the flow of solids down in the emulsion phase must increase. The increased downward velocity of the emulsion thus yields a greater drag force on the fuel particles, leading to a tendency for the particles to be at lower position in the bed. Owing to the tendency for fuel to be located in lower regions of the bed, a greater amount of fuel exiting the primary chamber is expected to be observed.

It should however be noted that for big slit heights, the amount of char gasification becomes quite insensitive to changes in fluidization velocity. This especially noticeable when comparing the $h_{slit} = 56.8cm$ case for the fluidization velocities of 1.2 and 1.4 m/s. This result suggest that there exist a threshold in the height of the slit at which the control of the novel concept by the means of altering the fluidization velocity, becomes inefficient.

6

Conclusion

A model describing the axial mixing in fluidized beds was developed and implemented into Chalmers three-dimensional mathematical model for commercial fluidized bed applications. The model development was especially directed towards mixing of biomass fuels and through simulations it has been seen that the model is able to capture many of the characteristics expected for biomass conversion processes. Such as the segregating behavior due to formation of endogenous bubbles

The simulations suggest that the kinetics of the biomass pyrolysis are of great importance for the mixing in the bed. For fuel particles of small initial diameter, the effect of the assumption of a constant pyrolysis time becomes apparent, as the simulations yields a significantly different behavior compared to larger fuel particle diameters. Further studies of the pyrolysis kinetics could thus offer valuable information that could be used for improvements to the developed model.

The novel multi-staging fluidized bed concept was evaluated with aid of the developed model. From simulations it was shown that the pressure difference, the height of the slit and fluidization velocity all had effects on the degree of char gasification occurring within the primary chamber. Furthermore, the results indicate that the pressure drop could be used as control parameter for controlling the retention time in the primary chamber.

It was also shown that the process could be controlled by varying the fluidization velocity. However, the ability to control the process with the fluidization velocity becomes very limited if the height of the slit is too large.

Bibliography

[1] Hartmann, D.L., A.M.G. Klein Tank, M. Rusticucci, L.V. Alexander, S. Brönnimann, Y. Charabi, F.J. Dentener, E.J. Dlugokencky, D.R. Easterling, A. Kaplan, B.J. Soden, P.W. Thorne, M. Wild and P.M. Zhai, 2013: Observations: Atmosphere and Surface. In: Climate Change 2013: The Physical Science Basis. Contribution of Working Group I to the Fifth Assessment Report of the Intergovernmental Panel on Climate Change [Stocker, T.F., D. Qin, G.-K. Plattner, M. Tignor, S.K. Allen, J. Boschung, A. Nauels, Y. Xia, V. Bex and P.M. Midgley (eds.)]. Cambridge University Press, Cambridge, United Kingdom and New York, NY, USA.

[2] Dominic Woolf, James E. Amonette,F. Alayne Street-Perrott, Johannes Lehmann, Stephen Joseph, Sustainable biochar to mitigate global climate change, Nature Communications, Volume 1, Issue 56, 2010.

[3] Cherubini, F. , Peters, G. P., Berntsen, T. , Stromman, A. H. and Hertwich, E. (2011), CO2 emissions from biomass combustion for bioenergy: atmospheric decay and contribution to global warming. GCB Bioenergy, 3: 413-426.

[4] Ke Zhao, Henrik Thunman, David Pallarès, Henrik Ström, Control of the solids retention time by multi-staging a fluidized bed reactor, Fuel Processing Technology, Volume 167, 2017, Pages 171-182.

[5] Daizo Kunii, Octave Levenspiel, CHAPTER 1 - Introduction, Editor(s): Daizo Kunii, Octave Levenspiel, Fluidization Engineering (Second Edition), Butterworth-Heinemann, 1991, Pages 1-13.

[6] Joris Koornneef, Martin Junginger, André Faaij, Development of fluidized bed combustion—An overview of trends, performance and cost, Progress in Energy and Combustion Science, Volume 33, Issue 1, 2007, Pages 19-55.

[7] A.A. Khan, W. de Jong, P.J. Jansens, H. Spliethoff, Biomass combustion in fluidized bed boilers: Potential problems and remedies, Fuel Processing Technology, Volume 90, Issue 1, 2009, Pages 21-50.

[8] David A. Tillman, 7 - FLUIDIZED BED COMBUSTION OF SOLID FUELS, Editor(s): David A. Tillman, Combustion of Solid Fuels & Wastes, Academic Press, 1991, Pages 319-372.

[9] Linghong Zhang, Chunbao (Charles) Xu, Pascale Champagne, Overview of recent advances in thermo-chemical conversion of biomass, Energy Conversion and Management, Volume 51, Issue 5, 2010, Pages 969-982.

[10] Prabir Basu, CHAPTER 3 - Fluidized Bed Gasification, Combustion and Gasification in Fluidized Beds (First Edition), CRC Press, Boca Raton,2006, Pages 59-97.

[11] Kristina Göransson, Ulf Söderlind, Jie He, Wennan Zhang, Review of syngas production via biomass DFBGs, Renewable and Sustainable Energy Reviews, Volume 15, Issue 1, 2011, Pages 482-492.

[12] J G Yates, CHAPTER 1 - Some fundamental aspects of fluidization, Editor(s): J G Yates, In Butterworths Monographs in Chemical Engineering, Fundamentals of Fluidized Bed Chemical Processes, Butterworth-Heinemann, 1983, Pages 4-71.

[13] I. Eames, M.A. Gilbertson, Mixing and drift in gas-fluidised beds, Powder Technology, Volume 154, Issues 2–3, 2005, Pages 185-193.

[14] Daizo Kunii, Octave Levenspiel, CHAPTER 5 - Bubbles in Dense Beds, Editor(s): Daizo Kunii, Octave Levenspiel, Fluidization Engineering (Second Edition), Butterworth-Heinemann, 1991, Pages 115-135.

[15] Kohler, Anna. Modelling axial mixing of char - application to the dense bottom bed in CFB boilers 12th International Conference of Fluidized bed Technology, May 2017, Krakow, Poland. Unpublished conference paper.

[16] F. Johnsson, S. Andersson, B. Leckner, Expansion of a freely bubbling fluidized bed, Powder Technology, Volume 68, Issue 2, 1991, Pages 117-123.

[17] Daizo Kunii, Octave Levenspiel, CHAPTER 6 - Bubbling Fluidized Beds, Editor(s): Daizo Kunii, Octave Levenspiel, Fluidization Engineering (Second Edition), Butterworth-Heinemann, 1991, Pages 137-164.

[18] Roberto Solimene, Antonio Marzocchella, Piero Salatino, Hydrodynamic interaction between a coarse gas-emitting particle and a gas fluidized bed of finer solids, Powder Technology, Volume 133, Issues 1–3, 2003, Pages 79-90.

[19] M. Fiorentino, A. Marzocchella, P. Salatino, Segregation of fuel particles and volatile matter during devolatilization in a fluidized bed reactor—I. Model development, Chemical Engineering Science, Volume 52, Issue 12, 1997, Pages 1893-1908.

[20] David Pallarès, Filip Johnsson, Macroscopic modelling of fluid dynamics in large-scale circulating fluidized beds, Progress in Energy and Combustion Science, Volume 32, Issues 5–6, 2006, Pages 539-569.

[21] H. K. Versteeg and W. Malalasekera. An Introduction to Computational Fluid Dynamics. The Finite Volume Method. Longman Group Ltd., London, 1995.

[22] Johanna Olsson, David Pallarès, Filip Johnsson, Lateral fuel dispersion in a large-scale bubbling fluidized bed, Chemical Engineering Science, Volume 74, 2012, Pages 148-159.

[23] Louise Lundberg, Robert Johansson, David Pallarès, Henrik Thunman, A conversion-class model for describing fuel conversion in large-scale fluidized bed units, Fuel, Volume 197, 2017, Pages 42-50.

[24] Keith Liadler, Robert Johansson, David Pallarès, Henrik Thunman, The Development of the Arrhenius Equation, Journal of Chemical Education, Volume 61, 1984, Pages 494-498.

[25] I. Petersen, J. Werther, Experimental investigation and modeling of gasification of sewage sludge in the circulating fluidized bed, Chemical Engineering and Processing: Process Intensification, Volume 44, Issue 7, 2005, Pages 717-736.

A

Appendix 1

In table A.1, values for parameter used in the model is presented.

Table A.1: Table displaying numerical values of parameters used in the model.

Variable	Description	Value
D_{Axial}	Axial fuel dispersion coefficient	0.001 m$^2/s$
$D_{Lateral}$	Lateral fuel dispersion coefficient	0.1 m$^2/s$
f_w	Wake fraction	0.22
f_w	Wake fraction	0.22
N_{char}	Number of char conversion classes	4
N_{Drydev}	Number of drying and devolatilization classes	3
p	Pressure level	101300 Pa
T	Temperature	1123K
X_C	Fuel carbon content	0.545
X_H	Fuel hydrogen content	0.0593
X_O	Fuel oxygen content	0.3922
X_N	Fuel nitrogen content	0.0032
X_S	Fuel sulphur content	0.0004
$Y_{Moisture}$	Fuel moisture content	0.486
$Y_{Volatile}$	Fuel volatile content	0.363
Y_{Char}	Fuel char content	0.123
Y_{Ash}	Fuel ash content	0.028
α	Impact factor for fuel in bubble phase	0.3